HOSTED BY
ELSEVIER
CrossMark
Available online at www.sciencedirect.com
ScienceDirect
Journal of Magnesium and Alloys 4 (2016) 306–313
www.elsevier.com/journals/journal-of-magnesium-and-alloys/2213-9567

Full Length Article

Correlation between microstructure and wear behavior of AZX915 Mg-alloy reinforced with 12 wt% TiC particles by stir-casting process

Nagaraj M. Chelliah [a], Harpreet Singh [a,*], M.K. Surappa [b]

[a] Department of Mechanical Engineering, Indian Institute of Technology Ropar, Rupnagar 140001, Punjab, India
[b] Department of Materials Engineering, Indian Institute of Science, Bengaluru 560012, Karnataka, India

Received 25 July 2016; revised 10 September 2016; accepted 16 September 2016
Available online 26 September 2016

Abstract

The present work concerns with correlation between microstructure and wear behavior of AZX915 Mg-alloy reinforced with 12 wt% of TiC particles by stir-casting process. Dry sliding tests were performed under ambient environment by using a pin-on-disc (EN8 steel) configuration with a normal load of 50 N at a constant sliding speed of 2.50 ms^{-1}. While as-cast composite experienced delamination wear, heat treated composite suffered from delamination and oxidation wear during dry sliding contact. Moreover, the heat treated composite exhibited lower friction and higher wear rate as compared to the as-cast composite. Friction and wear behavior were correlated with microstructures based on the concept of oxidation tendency and crack nucleation/propagation. Further, a schematic model has been proposed illustrating wear mechanisms from the point of view of subsurface microstructural evolution of the AZX915-TiCp composite.

Keywords: Mg-alloys; Magnesium matrix composites; Heat treatment; Delamination; Tribo-oxidation

1. Introduction

Being a light weight material, Mg-alloys [1–3] have significant potential to be employed in automotive and aerospace applications owing to high specific strength and reduced fuel consumption. AZ91 Mg-alloy exhibits excellent casting properties and room temperature mechanical strength; however, it is not well-suited for tribological application, especially when the friction temperature exceeds 150 °C [4]. Such inferior tribological performance emerges from the dissolution of β-$Mg_{17}Al_{12}$ intermetallic phase at the grain boundaries. The addition of calcium may enhance the high temperature tribological performance or creep properties of Mg–Al alloys [5]. Calcium favors precipitation of thermally stable intermetallics of Al_2Ca lava phase by suppressing the formation of low melting point intermetallics of β-$Mg_{17}Al_{12}$ phase [6]. It has been learned that the high temperature tribological performance of Mg-based alloys can be significantly improved by adopting metal matrix composite (MMCs) approach. MMCs are most commonly prepared by stir-casting process by which the variety of thermally stable ceramics such as SiC, TiC, and Al_2O_3 particles are physically mixed with the molten Mg-based alloys [7]. MMCs are capable of providing improved mechanical strength, wear resistance, high temperature creep resistance or dimensional stability when imposed to dynamic mechanical and thermal disturbances. Rashad et al. [8] investigated high temperature mechanical behavior of AZ61–3GNP composite fabricated using disintegrated melt technique [9,10]. They reported that fracture strain is enhanced at high temperature owing to significant grain refinement and uniform dispersion of GNPs in the magnesium matrix. Labib et al. [11] investigated dry sliding wear behavior of a Mg–SiCp composite at room and elevated temperatures. They observed that transition from mild to severe wear occurs at high load with increasing SiCp content in the magnesium matrix. Sharma et al. [12] also evidenced a similar trend after reinforcing AZ91 Mg-alloy with feldspar particles (composed of aluminosilicates of sodium, potassium, and calcium). Lim et al. [13] reported that wear rate of AZ91–SiCp composites is greater than that of unreinforced AZ91 Mg-alloy if delamination wear is predominant. They explained that high probability of de-cohesion at the interface between the ceramic particle and

* Corresponding author. Department of Mechanical Engineering, Indian Institute of Technology Ropar, Rupnagar 140001, Punjab, India. Fax: +91 1881 223395.
E-mail address: harpreetsingh@iitrpr.ac.in (H. Singh).

http://dx.doi.org/10.1016/j.jma.2016.09.002

the matrix material produces inferior wear response. However, Yao et al. [14] observed superior wear performance with AZ91-TiCp composite as compared to unreinforced AZ91 Mg-alloy during delamination wear. Such contradictory reports on the wear property of the MMCs can be understood better if the correlation between the microstructure and wear behavior is well-recognized. Both cast and wrought Mg-alloys are most often subjected to a variety of heat treatment techniques to enhance their mechanical properties as well as tribological characteristics. Effect of heat treatment on dry sliding wear behavior of AZ91-based MMCs has not been explored well. In fact, the dry sliding wear behavior of AZ91-based MMCs containing calcium has not been studied yet to the best of our knowledge.

Main objective of the current work is to understand the correlation between microstructure and wear behavior of AZX915–12TiCp composite under a dry sliding contact. Dry sliding operating parameters were chosen carefully in such a way that MMC experiences a friction temperature of above 150 °C within the domain of delamination wear. The idea behind the addition of calcium into AZ91 Mg-alloy melt prior to the reinforcement was to obtain high temperature stable Al_2Ca lava phase in the final microstructure of fabricated MMCs.

2. Experimental methods

2.1. Investigated materials

In the current study, die-cast AZ91C Mg-alloy was chosen as the matrix material. Chemical composition of this Mg-alloy is provided in Table 1. Calcium globules with a spherical diameter of 0.5 mm were used as an alloying element. Titanium carbide (TiC) particles with particle size in the range of 5–20 μm were chosen as the reinforcement phase.

2.2. Stir-casting process

Die-cast AZ91 Mg-alloy ingot was cut into small blocks followed by machining of their surfaces to remove any native oxide film. One kilogram of the machined blocks was melted in a steel crucible using an electrical resistance furnace and superheated to a temperature of 850 °C. In the mean time, calcium globules and TiC particles were pre-heated in a muffle furnace at a temperature of 150 °C and 400 °C respectively. The steel crucible was continuously purged with Ar–5%SF_6 gas mixture to eliminate the risk of flammability with magnesium. The melt was then mechanically stirred by a 3-axial stirrer blade at 600 rpm, in which the pre-heated calcium globules (5% by weight) were added. The stirring process was continued for another 5 min. Subsequently, the temperature of the molten alloy was reduced to 750 °C. In order to ensure homogeneous dispersion of TiC particles within the melt, an appropriate vortex was created at 650 rpm during stirring of the melt mixtures. The pre-heated TiC (12% by weight) particles were added into the melt, keeping the stirring operation continued for 10 min. Finally, the mixed molten slurry was bottom-poured into a pre-heated (at a temperature of 300 °C) cylindrical plain carbon steel mold. As-cast composite specimens were sectioned from the fabricated castings and machined to cylindrical pins; having a diameter of 6 mm and a length of 30 mm in order to perform dry sliding tests. Rectangular coupons, each measuring 26 mm × 5 mm × 2.5 mm with a notch of 1.5 mm, were cut from the composite castings using an electric discharge machine. These coupons were used for fracture toughness testing.

2.3. Heat treatment

To study the correlation between the microstructure and wear behavior, the fabricated MMCs was subjected to T4 heat treatment on composite specimens. T4 heat treatment was performed at a temperature of 420 °C under Argon environment for 48 hours. The as-cast and T4 heat treated specimens were designated as ac-AZX915/TiCp and ht-AZX915/TiCp, respectively.

2.4. Pin-on-disc tests

Dry sliding wear performance of the as-cast and heat treated pin specimens was evaluated using a pin-on-disc tribometer (CETR Instrument, DFH-100, USA). EN8 steel (with a diameter of 70 mm and a thickness of 5 mm) was used as the counter-face disk material. The specimens were properly cleaned with ethanol solution using an ultrasonicator for 10 min before the tribological tests. The dry sliding tests were performed at a constant sliding speed of 2.5 ms^{-1} with a normal load of 50 N for a sliding distance of 1500 m under ambient environment. The worn-out pins were weighed before and after each test run using single-pan electronics (a resolution of 0.1 mg). Wear debris particles were also collected after each test run for wear debris analysis. Wear rate for the tested specimens was quantified based on the difference in volumetric losses per unit sliding distance before and after the sliding tests. Friction force and normal force were continuously recorded by a load cell in order to evaluate coefficient of friction (COF) during sliding contact. Each of the tests was repeated three times to ensure repeatability in the friction and wear data, such that each reported value of COF and wear rate is an average of three observations.

2.5. Material characterization

Microstructures of the as-cast and heat treated composite specimens were analyzed by an optical microscope (Leica DM2700, Germany). Microstructures, worn-out surfaces,

Table 1
The typical chemical composition of as-received die-cast Mg-alloy.

Mg-alloy	Chemical composition (wt%)							
AZ91C	Al	Zn	Mn	Si	Fe	Cu	Ni	Mg
	8.3–9.7	0.3–1.0	0.15–5.0	0.1 Max	0.005 Max	0.03	0.002	Balance

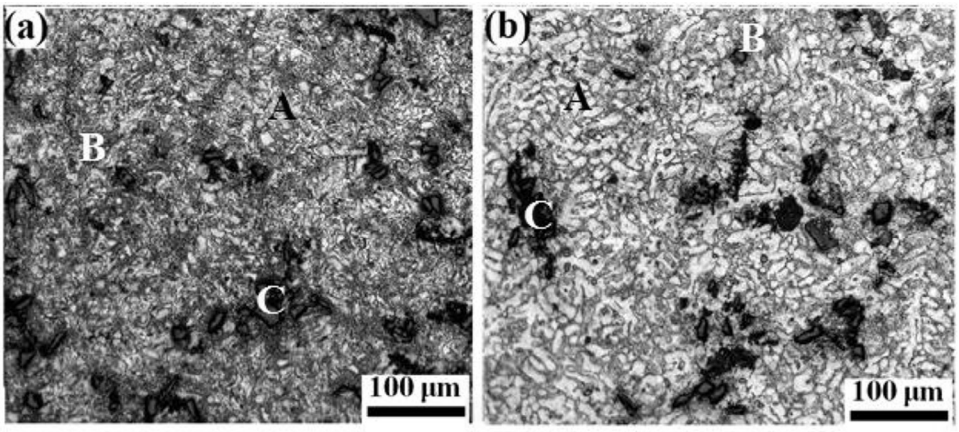

Fig. 1. Optical micrographs of the investigated specimen: (a) as-cast AZX915 composite and (b) heat treated AZX915 composite reinforced with 12 wt% of titanium carbide particles.

sub-surface regimes, and wear debris morphologies of the tested specimens were characterized by a scanning electron microscope (JEOL JSM-6610LV, Japan). Diffraction spectra were obtained to indentify various phases in as-cast/heat treated composite specimens and wear debris particles using an X-Ray Diffractometer (PANalytical X'pert-Pro (MPD), Netherlands). Micro-hardness Tester (Wilson Instrument, Model 401/402 MVD, UK) was used to evaluate Vickers microhardness of the investigated specimens at a load of 100 gf for a dwell time of 15 seconds. Fracture toughness of the composite specimens was also estimated in three point bending mode by Tinius Olsen universal testing machine. The fracture toughness (K_{IC}) was calculated using the following equations [15]:

$$K_{IC} = \left[\frac{P_f S}{B(W)^{\frac{2}{3}}}\right] f\left(\frac{a}{W}\right) \quad (1)$$

$$f\left(\frac{a}{W}\right) = 3\left(\frac{a}{W}\right)^{\frac{1}{2}}\left[1.99 - \left(\frac{a}{W}\right)\left(1-\frac{a}{W}\right)\left(2.15 - 3.93\frac{a}{W}\right)\right] \quad (2)$$

where P_f represents the load at fracture, S is the span of the composite specimen between load supporting positions, a is the length of the crack or size of the notch, and B and W indicate the thickness and width of the composite specimen, respectively.

3. Results and discussion

3.1. Microstructural evolution

Typical microstructures of the as-cast and the heat treated AZX915/TiCp composites are depicted in Fig. 1. Secondary intermetallic phases and reinforced ceramic particles can be easily distinguished in the matrix of composite materials as follows: light gray areas (marked as A) are primary α-Mg phase, whereas dark gray areas (indicated as B) are secondary intermetallic precipitates of β-$Mg_{12}Al_{17}$ or Al_2Ca phases, and black colored particles (marked as C) refer to TiCp particles. It is perceptible that the distribution of TiC particles is more or less uniform in the matrix of both the composites, as shown in Fig. 1(a) and Fig. 1(b). Microstructural evolution of the as-cast and the heat treated composites is shown in Fig. 2. It can be observed that the primary α-Mg phase (dark gray color regimes (A)) is surrounded by discontinuous network of secondary intermetallic precipitates (β-$Mg_{12}Al_{17}$ or Al_2Ca phases (B)) as shown in Fig. 2(a) and Fig. 2(b). It is clearly evident that TiCp (marked as C) particles are distributed within the grains and at

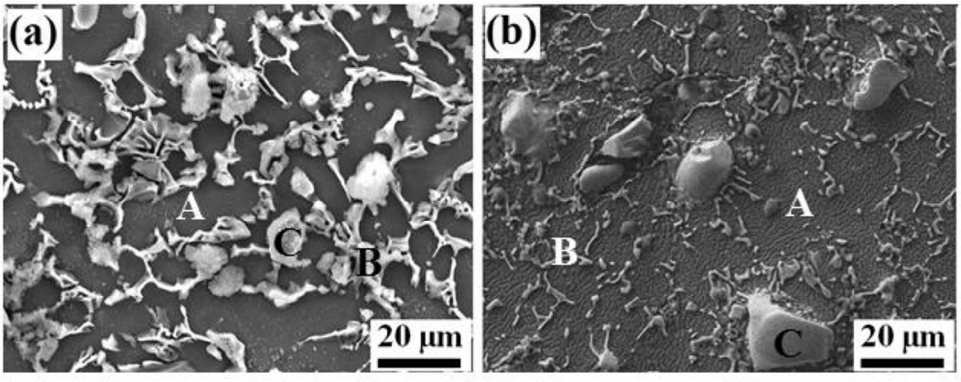

Fig. 2. SEM micrographs of the investigated specimen: (a) as-cast AZX915 composite and (b) heat treated AZX915 composite reinforced with 12 wt% of titanium carbide particles.

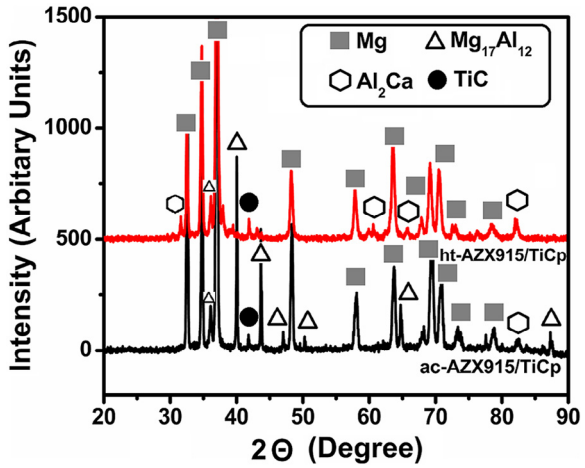

Fig. 3. XRD spectra of as-cast and heat treated AZX915–12wt%TiCp composites.

the grain boundaries of composite specimens. This suggests that TiCp particles are either engulfed or pushed away by the solidification front during the casting process [16]. It can be observed that the intensity of secondary phases decreases after the T4 heat treatment (compare Fig. 2(a) and Fig. 2(b)). This can be ascribed to the dissolution of β-$Mg_{17}Al_{12}$ phase during the T4 heat treatment process [17]. The striking difference in the microstructures of the as-cast and the heat treated composites is that the former contains dual secondary intermetallic precipitates of both β-$Mg_{17}Al_{12}$ and Al_2Ca phases, whereas the latter contains mainly of Al_2Ca phase with a marginal level of residual β-$Mg_{17}Al_{12}$ phase. Such difference in the microstructures could be verified from XRD spectra (Fig. 3). For instance, the intensity and number of Al_2Ca peaks are relatively higher in ht-AZX915/TiCp specimen when compared with those in ac-AZX915/TiCp specimen. On the other hand, most of β-$Mg_{17}Al_{12}$ peaks disappear in ht-AZX915/TiCp specimen. This scenario suggests that T4 heat treatment process favors the formation of Al_2Ca phase at the cost of dissolution of β-$Mg_{17}Al_{12}$ phase. Therefore, we believed that formation of Al_2Ca phase may occur at two different physical situations; (i) during casting process at a temperature below the liquidus temperature of the matrix material and (ii) during T4 heat treatment process at a temperature of 420 °C.

3.2. Correlation between microstructure and friction

According to the Bowdon and Tabor model [18], friction is composed of two physical components namely, ploughing and adhesion. While ploughing component arises from the degree of plastic deformation in the contacting surfaces, adhesion component emerges from adhesive force existing between the contacting surfaces. During sliding contact, coefficient of friction (i.e. ratio of frictional force to normal force) typically depends on various parameters such as surface roughness, material properties (elastic modulus and hardness), sliding speed, normal load, temperature and environment. It is a well-known fact that the adhesion component of friction can be reduced significantly if any lubricant or tribo-induced oxide

Table 2
Summary of data for AZX915–12TiCp composites.

Properties	ac-AZX915/12TiCp composite	ht-AZX915/12TiCp composite	Percentage change
Fracture toughness MPa · $m^{1/2}$	13.0 ± 2.1	7.5 ± 1.6	−42.30%
Microhardness (HV0.1)	106.67 ± 8.20	88.74 ± 5.93	−16.80%
Friction coefficient	0.30 ± 0.08	0.068 ± 0.03	−77.30%
Wear rate × 10^{-11}(m^3/m)	6.21 ± 0.37	12.99 ± 0.20	+109.17%

film is introduced. Moreover, such oxide films are produced on the metallic surfaces due to availability of friction heat if the metals have higher oxidation tendency. These oxide films can serve as a solid lubricant by preventing direct metal–metal contact which eventually tends to decrease the adhesive force and coefficient of friction.

From Table 2, it can be noticed that COF for ht-AZX915/TiCp decreases by 4.5 times in comparison with that of ac-AZX915/TiCp. This significant reduction in COF may be attributed to the phenomenon of tribo-oxidation. Czerwinski [19] observed that oxidation tendency of AZ91 Mg-alloy accelerates when temperature reaches above 437 °C. In accordance with friction-temperature model [20], estimated friction temperature experienced by ht-AZX915/TiCp specimen was 421 °C. This temperature is close to the temperature at which oxidation tendency in AZ91-based Mg-alloy accelerates. It is worthwhile to correlate the microstructures of investigated composites with their oxidation tendency. As mentioned earlier, ht-AZX915/TiCp specimen possesses a meager amount of β-$Mg_{17}Al_{12}$ phase when compared to that in ac-AZX915/TiCp specimen. It is already reported that the presence of β-$Mg_{17}Al_{12}$ phase enhances the corrosion or oxidation resistance of AZ91 Mg-alloy owing to high cathodic potential [21,22]. In other words, ht-AZX915/TiCp specimen having meager amount of β-$Mg_{17}Al_{12}$ phase tends to oxidize easily as compared to ac-AZX915/TiCp specimen. As shown in Fig. 4, it is revealed that the magnitude of MgO peaks is intensified in ht-AZX915/TiCp specimen in comparison to that in ac-AZX915/TiCp.

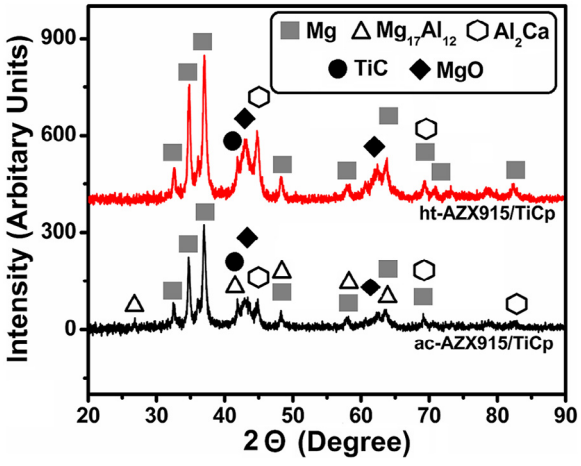

Fig. 4. XRD spectra of the collected wear debris particles slid at 2.5 ms^{-1} with normal load of 50 N.

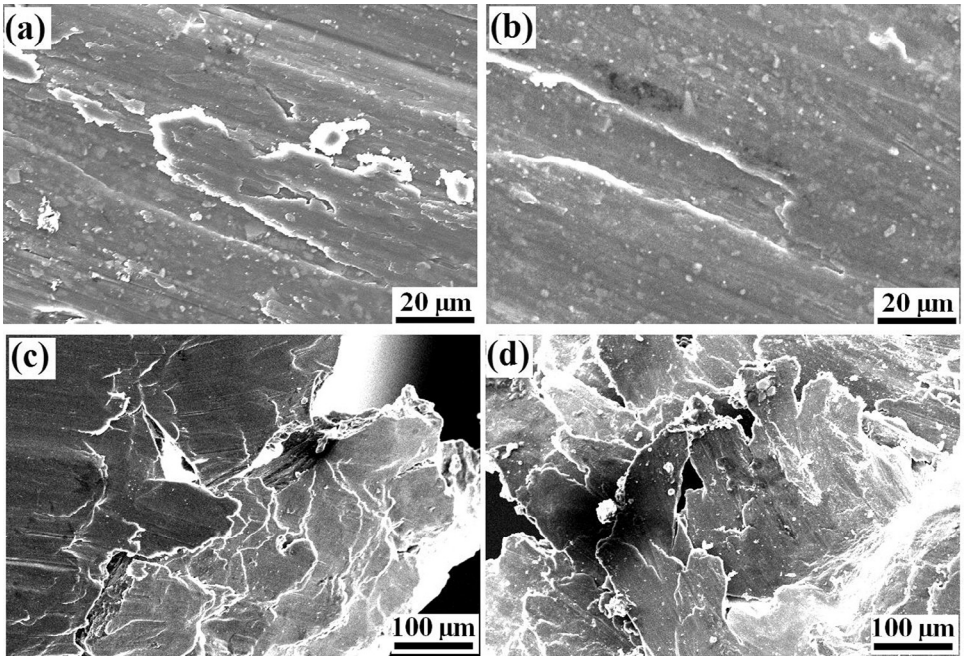

Fig. 5. Worn surfaces of the investigated specimen slid at 2.5 ms^{-1} with normal load of 50 N; (a) and (c) as-cast AZX915 composite; (b) and (d) heat treated AZX915 composites reinforced with 12 wt% titanium carbide particles.

Under similar dry sliding conditions, the microstructures with different levels of β-$Mg_{17}Al_{12}$ phase show disparity in their tendency toward oxidation and tribo-oxidation. This strong correlation between the microstructure and tribo-oxidation indicates that there exists a relation between the microstructure and COF. In order to validate this hypothesis, the dry sliding tests were also performed on unreinforced AZX915 Mg-alloys. COFs of as-cast and heat treated AZX915 Mg-alloy specimens were evaluated as 0.41 and 0.096 respectively. When compared with unreinforced AZX915 Mg-alloy, COF of the composite specimens got reduced by 56% and 42% for the as-cast and heat treated conditions respectively. Further, Cheng et al. [23] pointed out that oxide film of Ca-bearing AZ91 alloy is usually thicker, more brittle and tends to break away easily when imposed to thermal cycles. As long as the rate of formation of oxide film is greater than the rate of removal of oxide film, the tribo-induced oxide (MgO) film can serve as an effective solid lubricant, which eventually leads to lower COF in sliding contact. In the present work, the contribution of adhesion to friction seems to be reduced significantly. This negligible adhesion is mainly associated with the formation of tribo-induced oxide film (MgO) which can suppress the direct metal–metal contact and subsequent adhesive forces. In addition, the worn surfaces of ht-AZX915/TiCp specimen indicate no signs of material transfer and surface melting in sliding contact (see Fig. 5(a) to Fig. 6(b)). Hence, it is expected that friction coefficient shall be predominantly controlled by the degree of plastic deformation.

The simplified theory of friction proposed by Bowdon and Tabor is given by the following relation [18]:

$$\mu \approx \frac{\tau_i}{2.8\,Y} \tag{3}$$

where μ is the coefficient of friction, τ_i is the shear strength and Y is the flow pressure or hardness of the material. The equation suggests that friction coefficient inversely scales with the

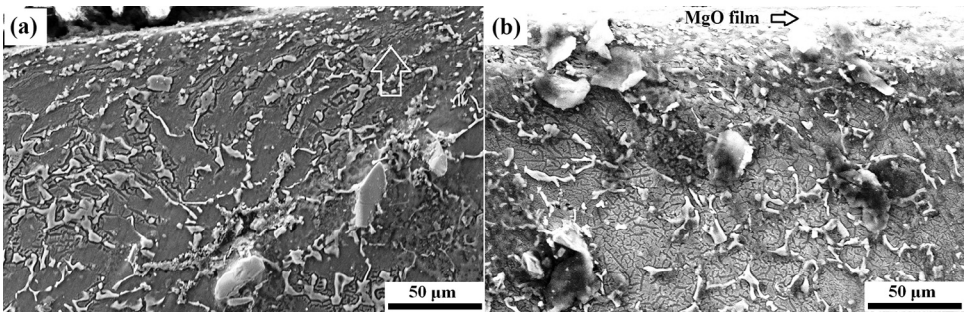

Fig. 6. Subsurface zone of the investigated specimen slid at 2.5 ms^{-1} with a normal load of 50 N; (a) as-cast AZX915 composite, (b) heat treated AZX915 composites reinforced with 12 wt% titanium carbide particles.

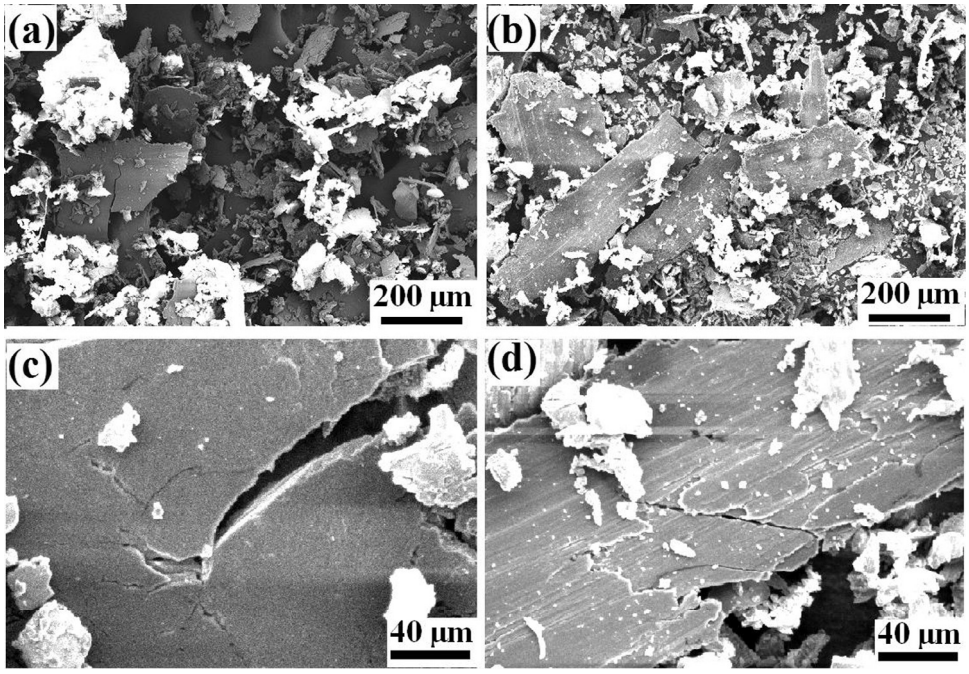

Fig. 7. Wear debris particles of the investigated specimen slid at 2.5 ms^{-1} with normal load of 50 N. (a) and (c) as-cast AZX915 composite; (b) and (d) heat treated AZX915 composites reinforced with 12 wt% titanium carbide particles.

hardness of the material. Materials with higher hardness experience minimal degree of plastic deformation and thus show lower µ. However, tribological data show a contradictory response as shown in Table 2. For instance, ac-AZX915/TiCp with high micro-hardness exhibits larger COF when compared to ht-AZX915/TiCp specimen. Though experimental results seem to be contradictory, the clear insight can be obtained only after the detailed investigation of the worn surfaces and subsurfaces. Nevertheless, the existence of tribo-oxidation weakens the correlation between hardness and friction. In summary, the strong correlation between the microstructure and friction coefficient based on the concept of oxidation tendency appears to be valid for the investigated composite specimens.

3.3. Correlation between microstructure and wear behavior

Suh [24] developed the delamination theory of wear to explain the wear of surfaces in sliding contact. He describes the sequential events for the production of laminate wear debris as follows: (i) when two surfaces come into contact, normal and frictional forces are transmitted through their contact points or asperities; (ii) the surface traction exerted by the harder asperities induces incremental plastic deformation on the softer materials with repeated loading; (iii) as the subsurface deformation continues, cracks are nucleated below the surface or de-cohesion occurs at the interface between secondary particle and the matrix material; (iv) subsequent repeated loading and subsurface plastic deformation causes the cracks to extend and propagate parallel to the surface; and (v) when these cracks finally shear to the free surface, long and thin or thick laminated wear debris are produced. In order to achieve de-cohesion, the shear stress induced by sliding contact must exceed the interfacial shear strength between the secondary particle and the matrix material [24]. The depth of crack nucleation and distance of propagation typically depends on the material properties, normal load and friction characteristics of the surface.

SEM micrographs of worn surfaces of the investigated specimens are shown in Fig. 5. Existence of sheet-like features and crater patterns on the worn surfaces indicates the existence of delamination wear in both the as-cast (Fig. 5(a)) and the heat treated specimens (Fig. 5(b)). In Fig. 5(c), wavy pattern of compacted thin sheets at trailing edge of ac-AZX915/TiCp specimen suggests that the degree of plastic deformation is intensified in the subsurface zone during delamination wear. On the other hand, ht-AZX915/TiCp specimen underwent lesser plastic deformation during delamination wear as the detached subsurface layers are featured by brittle fracture patterns as could be seen in Fig. 5(d). Subsurface microstructures of the investigated pin specimens are depicted in Fig. 6. As shown in Fig. 6(a), the existence of curved deformation bands (indicated by arrow) along the sliding direction suggests that significant plastic deformation occurs in the subsurface zone of as-cast specimen. In Fig. 6(b), existence of charged oxide layer in near surface region of the heat treated composite provides evidence for tribo-oxidation wear. Analyses of worn surfaces and subsurface in Fig. 5(a) to Fig. 6(b) revealed that while the as-cast composite experiences delamination wear, the heat treated composite promoted delamination and oxidation wear during dry sliding contact.

Fig. 7 illustrates surface morphologies of the collected wear debris. As shown in Fig. 7(a), ac-AZX915/TiCp composite specimen produced wear debris with more or less irregular plate-like morphologies with an average size of around 50 µm.

In Fig. 7(b), wear debris of ht-AZX915/TiCp specimen can be categorized into two types of morphologies as follows: (i) elongated or irregular shaped wear debris with a wide range of size distribution having length varying from 500 μm to 1 μm; such wear debris are usually produced by the delamination process; (ii) near-spherical or equi-ax shaped and fine-sized wear debris particles (1 to 10 μm). These wear debris are predominantly generated by tribo-oxidation. The dominance of tribo-oxidation wear is also supported by the presence of MgO peaks in the XRD spectrum (Fig. 4). It is pertinent to mention that though ht-AZX915/TiCp specimen exhibits higher wear rate, it shows less friction coefficient. This means that tribo-induced oxide layer seems to be thicker but brittle in nature.

Table 2 shows that ht-AZX915/TiCp specimen exhibits higher wear rate in comparison with the ac-AZX915/TiCp specimen. The higher wear rate of the heat treated specimen can be explained on the basis of oxidation wear theory, similar to friction. As mentioned earlier, a meager presence of oxidation resistant β-$Mg_{17}Al_{12}$ phase leads to enhance the oxidation tendency in ht-AZX915/TiCp specimen. Further, the availability of thermal energy due to friction heat (friction temperature of 421 °C) accelerates the formation of brittle MgO film, which eventually tends to increase the wear rate in sliding contact.

Friedrich [25] proposed an empirical wear model which correlates wear rate of composite materials with their mechanical properties. They mentioned that wear rate of composite materials inversely scales with fracture toughness. Such correlation is given by the following formula:

$$\text{Wear rate } \alpha \ \frac{H^{1/2}E}{K_{IC}^2} \tag{4}$$

where F is a function of applied load, volume fraction and size of the reinforced particles and H, E and K_{IC} denote the hardness, elastic modulus and fracture toughness of the composite materials, respectively. In Table 2, it is evident that wear rate of composites decreases with increasing fracture toughness. This is consistent with an empirical wear model proposed by Friedrich [25].

In delamination wear, wear rate of composite material is controlled by rate of crack nucleation and propagation in the subsurface [24]. It is expected that the intensity of crack nucleation may be limited in ac-AZX915/TiCp specimen due to the fact that the applied load is shared by hybrid particles such as β-$Mg_{17}Al_{12}$, Al_2Ca and reinforced TiCp. In addition, the path of crack propagation could be interrupted or deviated by the existence of these hybrid particles in the subsurface. Kumar and Curtin [26] reviewed the significance of crack interaction with microstructure for various multiple phase alloys. They mentioned that cracks experience significant resistance while crossing the boundary of interface of intermetallics. We have preferred to analyze the path of crack propagation within single wear debris rather than the subsurface of the bulk specimen. This was due to the fact that cracks are most often enclosed or disappear during the specimen preparation stage itself (i.e. mechanical polishing). As shown in Fig. 7(c), it is evident that the path of crack propagation seems to be relatively unidirectional in the ht-AZX915/TiCp specimen. On the other hand, the crack path is featured by multiple branches in the ac-AZX915/TiCp specimen (Fig. 7(d)). It may be possible that the dissolution of β-phase occurs in the subsurface of as-cast specimen while the friction temperature reaches 421 °C. If dissolution of β-phase takes place, then its role on diverting the path of crack propagation is questionable. Under chosen dry sliding condition, total time available between two contacting surfaces is 600 s. Within this short interval, complete dissolution of β-phase in near surface region is not feasible. In order to validate this hypothesis, literature data regarding the time for dissolution of β-phase in AZ91 Mg-alloy were carefully reviewed. Zhu et al. [27] reported that minimum time required to dissolve 5 wt% of β-phase in AZ91 Mg-alloy at a temperature of 420 °C is 2400 s. Hence, the argument on the dissolution of β-phase during sliding contact could be ruled out. Based on experimental evidence, the microstructures of the investigated composites can be correlated with their wear properties as follows: (i) existence of hybrid phases in as-cast AZX915/TiCp composite offers better fracture toughness by suppressing the rate of crack nucleation or by deviating the path of crack propagation and thus tends to minimize the wear rate; (ii) the dissolution of β-$Mg_{17}Al_{12}$ phase during T4 heat treatment in the heat treated AZX915/TiCp composites tends to enhance the oxidation tendency, leading to the formation of brittle MgO film, which eventually results in higher wear rate. For comparative analysis, dry sliding wear behavior of unreinforced AZX915 Mg-alloy was also investigated. When compared to unreinforced AZX915 Mg-alloy, wear rate of composite specimen decreases by 47% and 33% for the as-cast and heat treated conditions respectively.

A schematic model illustrating wear evolution from the point view of microstructures of the investigated AZX915/TiCp composites is proposed in Fig. 8. It can be seen that crack is initiated by de-cohesion at the matrix/reinforcement interface. The path of crack propagation is predominantly deviated in the as-cast composites in comparison with that in the heat treated composites, through zig-zag configuration due to the existence of hybrid particles. Moreover, the intensity of formation of

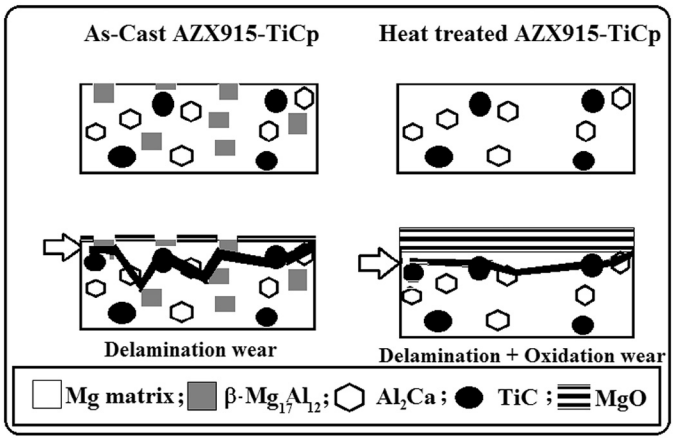

Fig. 8. Schematic representation of proposed geometrical model depicting the correlation between microstructure and wear property in AZX915–12wt%TiCp composites.

MgO scale is significantly enhanced in the heat treated composites as there is no β-$Mg_{12}Al_{17}$ phase to resist tribo-oxidation during sliding contact.

4. Conclusions

1. Under the chosen dry sliding conditions, wear rate of as-cast AZX915–12TiCp composite is primarily controlled by delamination wear, whereas the same is governed by the combination of tribo-oxidation and delamination in the case of heat treated AZX915–12TiCP composite.
2. Coefficient of friction for the heat treated AZX915–12TiCp composite decreased by 4.5 times in comparison with that of the as-cast composite. This is attributed to increase in the intensity of oxidation tendency in the former due to the dissolution of oxidation barrier β-$Mg_{17}Al_{12}$ phase.
3. Wear rate of the as-cast AZX915–12TiCp composite decreased by 2 times in comparison with that of the heat treated composite, which is associated with the existence of dual intermetallic precipitates of β-$Mg_{17}Al_{12}$ and Al_2Ca phases in the former which interrupt the path of crack propagation in the subsurface.
4. A schematic model has been proposed representing wear mechanism in the AZX915 composites from the point of view of subsurface microstructural evolution during sliding conditions.
5. T4 heat treatment was found to be deleterious for the AZX915–12TiCp composite with regard to its wear resistance.

Acknowledgments

The authors would like to express their gratitude to Mr. Ram Kumar and Mr. Amit Kaushal for their technical assistance in conducting tribological tests and XRD characterization respectively.

References

[1] B.L. Mordike, T. Ebert, Mater. Sci. Eng. A 302 (2001) 337–345.
[2] E. Aghion, B. Bronfin, Mater. Sci. Forum 19 (2000) 350–351.
[3] H. Friedrich, S. Schumann, J. Mater. Proc. Tech. 117 (2001) 276–281.
[4] D.S. Mehta, S.H. Masoodand, W.Q. Song, J. Mater. Proc. Tech. 155 (2006) 919–932.
[5] D. Amberger, P. Eisenlohr, M. Goken, Mater. Sci. Eng. A 510–511 (2009) 398–402.
[6] A.V. Koltygin, V.E. Bazhenov, E.A. Belova, A.A. Nikitina, J. Mag. Alloys. 1 (2013) 224–229.
[7] J. Hashim, L. Looney, M.S.J. Hashmi, J. Mater. Proc. Tech. 92–93 (1999) 1–7.
[8] M. Rashad, F. Pan, D. Lin, M. Asif, Mater. Des. 89 (2016) 1242–1250.
[9] M. Rashad, F. Pan, M. Asif, Mater. Sci. Eng. A 649 (2016) 263–269.
[10] M. Rashad, F. Pan, A. Tang, M. Asif, Prog. Nat. Sci. Mater. Inter. 24 (2014) 101–108.
[11] F. Labib, H.M. Ghasemi, R. Mahmudi, Wear 348–349 (2016) 69–79.
[12] S.C. Sharma, B. Annand, B.M. Krishma, Wear 241 (2000) 33–40.
[13] C.Y.H. Lim, S.C. Lim, M. Gupta, Wear 255 (2003) 629–637.
[14] J. Yao, W. Li, L. Zhang, F. Wang, M. Xue, H. Jiang, et al., Tri. Lett. 38 (2010) 253–257.
[15] R. Papirno, H.C. Weiss, Standard Test for Plane Strain Fracture Toughness of Metallic Materials: ASTM E-399, American Society for Testing and Materials, Philadelphia, 1989.
[16] M.K. Surappa, J. Mater. Proc. Tech. 63 (1997) 325–333.
[17] G.R. Ebrahimi, A. Maldar, R. Ebrahmi, A. Davoodi, Kov. Mater. 48 (2010) 277–284.
[18] F.P. Bowden, D. Tabor, The Friction and Lubrication of Solids, Oxford University Press, Oxford, 1950.
[19] F. Czerwinski, Acta Mater. 50 (2002) 2639–2654.
[20] J. Zhang, A.T. Alpas, Acta Mater. 45 (1997) 513–528.
[21] G. Song, Corr. Sci. 49 (2007) 1696–1701.
[22] J.D. Majumdar, U. Bhattacharya, A. Biswas, I. Manna, Surf. Coat. Tech. 202 (2008) 3638–3642.
[23] S. Cheng, G.-C. Yang, J.-F. Fan, Y.-J. Li, Y. Zhou, Trans. Non-Ferr. Met. Soc. China 19 (2009) 299–304.
[24] N.P. Suh, Wear 44 (1977) 1–16.
[25] K. Friedrich, Friction and Wear of Polymer Composites, Elsevier Science Publishers, Amsterdam, 1986, pp. 258–281.
[26] S. Kumar, W.A. Curtin, Mater. Today 10 (2007) 34–44.
[27] T. Zhu, Z.W. Chen, W. Gao, J. Mater. Eng. Perform. 19 (2010) 860–867.